AZIMUTHAL BRIGHTNESS VARIATIONS IN SATURN'S RINGS

H. J. Reitsema and R. F. Beebe

Department of Astronomy

New Mexico State University

Las Cruces, New Mexico 88003

and

B. A. Smith

Department of Planetary Sciences

University of Arizona

Tucson, Arizona 85721

(Received 5 September 1975)

Running Title: Saturn's Rings

Send proofs to: Harold J. Reitsema
Department of Astronomy
Box 4500
New Mexico State University
Las Cruces, New Mexico 88003

ABSTRACT

Azimuthal variations in brightness in the rings of Saturn have been studied on recent photographs. A ring brightness model has been developed which is used in conjunction with a two-dimensional numerical smearing process to investigate the effects of seeing and instrumental smearing on the data.

The results of this investigation show that the two ansae of the rings are of equal brightness. Furthermore, the observed surface brightness of Ring B, decreasing from the ansae towards the minor axis of the ring ellipse, can be fully accounted for as a result of smearing processes on an initial intensity distribution which is independent of azimuthal angle. In contrast, Ring A shows a roughly sinusoidal variation in brightness with minima in the quadrants following geocentric conjunctions and maxima in the others. The smearing is approximately removed from Ring A to yield the intrinsic surface brightness of the ring.

INTRODUCTION

This analysis is a detailed study of the surface brightness of the two brighter rings of Saturn. Our results confirm brightness variations in Rings A and B as reported by Camichel (1958), Ferrin (1974), and Price and Baker (1975) and suggest that the rings contain a significant population of large gravitationally-locked synchronously rotating particles. The maximum apparent brightness of Ring B increases from the minor axis towards each ansa, causing the ansae to be nearly 6 percent brighter than the ring near the planet. In the region where the ring passes over the planet the brightness is nearly constant. This variation is similar to the expected effect of atmospheric and photographic smearing. Ring A exhibits a more complex behavior. One pair of opposing quadrants in Ring A is bright, while the other pair is relatively dark. This brightness variation is always oriented such that the first quadrant (in which the ring particles, in their orbital motion, are approaching the eastern ansa) is dark. The effect, amounting approximately to a 10 percent modulation in the brightness of Ring A, did not change its nature over the period 1942 to 1957 for which Camichel had observations, and is still the same. These azimuthal brightness variations do not show any dependence on solar phase angle. Although they are the same for positive and negative ring plane inclination angles, Camichel's data indicated that the variation of Ring B increased as the ring opening decreased.

We have re-examined this problem using well-calibrated high-resolution photographic images obtained by the NMSU planetary photography program. Through application of computerized data reduction we have been able to obtain detailed descriptions of the brightness variations.

I. OBSERVATIONS

Calibrated patrol photographs of Saturn have been obtained at NMSU for all recent apparitions of Saturn using the f/75 focus of the 61-cm reflector at the Tortugas Mountain facility. A total of 20 plates from six nights was selected to give a reasonable sample of data over a range of phase angle before and after opposition and covering the spectrum from photographic infrared to ultraviolet. A summary of the data is contained in Table I.

Each plate consists of approximately sixteen images and a calibration step wedge. Calibration consists of 11 steps with exposure ratios of approximately $\sqrt{2}$ illuminated by a quartz-iodide lamp through the same type of filter used in the exposure of the planet.

The best image on each plate was digitized with the microphotometer of Sacramento Peak Observatory. Each image was aligned by fiducial marks so that the scan direction was parallel to the major axis of the rings. The scanning aperture was a 50 μm square and the output voltage was recorded at 40 μm intervals, producing a rastor pattern of 150 parallel scans of 300 data points each. The photometer output from the image scans and the scans of the calibration strip was recorded on magnetic tape.

Processing of the recorded data was carried out with the IBM 360 model 65 computer of the NMSU Computer Center. Conversion of the data from voltage to intensity was accomplished using the procedure of Beebe (1976), in which the calibration data are fitted to an analytic function. Using this function, the digital image was converted point by point to intensity.

In order to examine specific points in digital images, it is necessary to locate the position and orientation of the image in the data array. This can be a particularly difficult task when working with planetary images since, in general, one of the limbs will not be visible because of the solar phase angle. This problem, however, is easily overcome in the case of Saturn because the outer edge of the ring system is a sharp boundary which can readily be identified in the digital image.

The shape and dimensions of the ring ellipse were fixed by the accurately known plate scale of the Tortugas telescope and the geometric data on the rings contained in the American Ephemeris and Nautical Almanac. Hence, the transformation from the data array coordinate system to an image coordinate system required only the determination of the precise image center and orientation angle. In order to find the center of the image each scan was examined for the point at which the ring was first encountered and for the point at which the scan left the other side of the ring. These two positions were averaged to give the midpoint of the image in that scan. This process was repeated for each scan, and the resulting set of points were fitted with a linear function by least squares. Next, this procedure was repeated for vertical columns in the data grid to obtain another, nearly perpendicular, line. The intersection of these lines was adopted as the center of the image.

The lines obtained in this manner very nearly corresponded to the minor and major axes of the ring ellipse and were used as a first approximation for the orientation of the image in the array. A correction to this orientation angle was then determined. For each of 600 equally-spaced angular intervals, the computer searched for the position of maximum intensity of Ring B. The set of points for which the maximum was visible

was then compared with the peak position predicted by the current orientation angle and center. An adjustment was determined for the orientation angle through use of the linearized first-order difference equation,

$$d_i^2 = 2r_i^2 \sin\theta_i \cos\theta_i \,(1 + \sin^2 B)\,\Delta\phi$$

$$+ 2r_i(\cos^2\theta_i + \sin^2\theta_i \sin^2 B)\,\Delta r$$

in which (r_i,θ_i) are the polar coordinates of the i-th point in the rings and d_i^2 is the difference between the squares of the radii of the observed and predicted maxima in the direction θ_i. The orientation angle correction $\Delta\phi$ was found by least squares inversion of this equation. The parameter Δr was included to free the solution from the effects of errors in the presumed radius of maximum intensity. These adjustments were quite small and the process converged rapidly.

A computer program was written to facilitate examination of the ring brightness. Two modes of operation are available. The first produces a linear scan through the center of the image at any selected angle to the major axis of the ring system. In particular, this mode was used to plot the major axis ring profile. The other mode of operation reads the image intensity at a selected radius in the rings and plots this data as a function of the ring particle orbital angle. In order to enhance the visibility of any brightness variations, this mode also plots the deviation of the elliptical scan from the average ring brightness for that scan (see Figs. 1 and 2).

An examination of the linear scans through the image provided a sensitive test of the image centering. When the proper center and orientation of the image was determined, the outer ring boundaries were equidistant from

the center of the scan. The orientation of the image was further checked by comparing the length of scans made at equal angles on each side of the major axis. Only when the proper orientation was achieved were these lengths the same. From the behavior of the data during these operations and from subsequent work with the images we conclude that the orientation angle of the images has been determined to within ±3 arc minutes. The center of the images is similarly found to be accurate within ±0.3 data elements. The combined effects of these errors in centering and orientation do not exceed 0.1 arc seconds in the original image.

In order to examine the reliability of the photometric calibration of the data, four red plates from a single night were independently reduced and compared by measuring the two maxima of Rings A and B on the major axis of each image. The agreement among the various measures of Rings A or B indicates that the standard deviation of intensity from the mean profile is at the three percent level. This figure includes all photometric uncertainties caused by the photographic and reduction processes. The relative intensities of points in a single image should be more reliable than this because processing errors would be minimized. Thus, three percent is a conservative estimate of the reliability of observed relative brightness variations.

II. PHOTOMETRIC RESULTS

A. Ring B

The scans in the ring plane at a fixed radius in Ring B confirm the presence of a brightening in the rings from the minor axes to the ansae. Figure 1 is representative of a scan for Ring B. The abscissa has its origin at the point of superior geocentric conjunction and increases in the direction of ring orbital motion. Both the original data and a plot

of the deviation of intensity from the average intensity for the scan are shown. The average was computed using only points which did not appear in projection either in front of or behind the planet, and excluding points within the shadow of the planet on the rings. This scan was made at a radius which was 0.805 of the radius of the outer edge of Ring A and is thus near the maximum intensity of Ring B.

The ring is brightest at each ansa and decreases towards the minor axis. When the ring crosses the planet the observed surface brightness is nearly constant. This variation of brightness with azimuthal angle has been noted by others (e.g. Camichel (1958), Ferrin (1974)) and, as will be shown in Section III, is almost certainly an artifact caused by smearing due to seeing effects.

We observe this effect to be present in all of the images which we have examined. The average magnitude is a 6 percent enhancement from the minor axis to the ansae with the standard deviation of a single image being 1.4 percent. No correlation of the amplitude with color or phase is observed. Our data are too limited to permit an investigation of a possible correlation with ring-plane inclination to the line of sight.

The linear scans along the major axis of each image were examined for a possible systematic east-west asymmetry in Ring B as reported by Morrison (1974). No difference was found. The mean ratio of the maximum ring intensity in the west ansa to the east for all images was 1.001 ± 0.006.

B. Ring A

The brightness variations in Ring A are more complex than those in Ring B. Figure 2 shows the variation in surface brightness for this ring. As ring particles emerge from superior geocentric conjunction

they darken, reaching a minimum at an orbital phase angle near 50° and then brighten rapidly to a maximum near 110° and then darken slowly. This behavior is repeated as the ring particles pass inferior geocentric conjunction. The planet is seen through the ring where it crosses the disk. As a check of the reality of this observed variation, we examined the behavior of the scattered light by obtaining data scans at a fixed radius just outside of Ring A. These tracings showed that the scattered light does not share the assymetric behavior of Ring A. Thus the observed brightness variation appears to result from intrinsic ring variations rather than from the effects of such processes as vignetting, instrumental astigmatism, or atmospheric refraction.

Measures of the amplitude of this variation show it to be about 9 or 10 percent of the mean brightness of Ring A. The minima occur at orbital phase angles of 50° and 230° and the maxima appear at 110° and 290° with uncertainties of about 5 degrees. This places the observed maxima at approximately 20° and the minima at about 40° from the major axis when measured in the sky plane.

III. RING MODELS

It is well known that the peculiar geometry of the ring system causes large apparent brightness variations within the image due to the effects of atmospheric and photographic smearing. The rings appear broad at the ansae but the foreshortening due to the inclination of the rings causes the smearing near the minor axis to be much more severe than it is along the major axis. Previous studies of the effects of smearing on the ring image have been confined to one-dimensional analyses (Franklin and Cook (1965), Coupinot (1973), Lumme (1975)) and are therefore restricted to profiles along the axes of the ring ellipse.

To investigate the point-to-point variation in surface brightness we required a means of smearing a two-dimensional ring model along a fixed radius in the ring plane for comparison with the observational data. We have written a computer program which performs a two-dimensional smearing with a Gaussian shape on a ring model having an assumed brightness profile. For the point at which the smeared intensity value is to be computed, we use the assumed brightness in the model ellipse at 64 equally-spaced angular intervals (θ_j) along each of 20 concentric circles (r_i). The values are averaged and multiplied by the Gaussian coefficient at r_i and by a weighting factor related to the differential area in the annulus represented by the circular sample of points. The smeared intensity may be expressed as

$$I(x,y) = B \sum_{i=1}^{20} A_i \, e^{-h^2 r_i^2} \sum_{j=1}^{64} I(r_i,\theta_j)$$

where A_i is the area of the i-th annulus and B a normalizing factor. Thus, a numerical integration under a Gaussian point-spread function is achieved. This circularly symmetric sampling of data points used in the integration was chosen to avoid the assignment of a preferential direction to the point spread function. The radii of the sample circles are scaled to give adequate sampling for any selected resolution size. The natural resolution parameter in this procedure is the e^{-1} halfwidth of the Gaussian which is the reciprocal of the precision modulus h.

The true brightness profile of the rings of Saturn is not well known. While attempts have been made by several groups to deconvolve the observed brightness distribution (Cook, Franklin and Palluconi (1973), Coupinot (1973)), the results have not been entirely satisfactory. Probably the

least subjective approach is that of Franklin and Cook (1965), which divides the rings into ringlets of uniform brightness. Using three ringlets in Ring B and two in Ring A, they adjusted the relative intensities to give agreement with observation when the rings were smeared with an assumed smearing function.

We have followed a similar procedure and have converged on the ring divisions and intensities given in Table II. The positions and relative intensities of the ringlets were adjusted to give agreement with our observations in scans of the major axis of the plate B13447. A ramp has been included to represent Ring C and a representation of the planet itself was included to indicate qualitatively its effect on the observations of the rings where they are in proximity to, or crossing, the disk of the planet. We find, in agreement with Lumme (1975), that assigning the Cassini division an intensity equal to 0.24 of the maximum intensity in Ring B permits better agreement than does a completely black Cassini division. The initial attempts to match the observations indicated that the ring diameter in the American Ephemeris and Nautical Almanac was too small by about one-half percent. The diameter given by Reese (1972) was therefore used and gave satisfactory agreement.

Unfortunately, this process of matching a presumed ring profile to the observed profile is dependent upon the resolution parameter used for the smearing operation. An independent estimate of the magnitude of the smearing may be derived from the sharpness of the outer edge of the rings, but it is not certain that the outer boundary is intrinsically abrupt. The edge of the shadow cast by the planet on the rings at large phase angles is indeed abrupt, but here deconvolution of the observed profile

is made difficult by light scattered from the planet. From these two approaches we derived an initial estimate for the smearing half-width of 0.75 arc seconds. The final combination of ring profile and smearing function yielded an estimated half-width of 0.5 arc seconds for the seeing smear in the photographic image. The resulting computed ring profile is shown in Fig. 3 along with an observed major axis scan.

An investigation was made of the effects of seeing in the observed orbital angle dependence of the ring surface brightness wherein the ring model was smeared at a constant radius coincident with the maximum of Ring B. The resulting smeared scan of the model showed a behavior identical to that of the observed data. The predicted surface brightness fell by 6 percent from the ansae to points 70° away in the ring plane. This figure proved to be little influenced by the precise form of the assumed ring profile provided that the smeared major axis scan gave good agreement with the observations. The quantity

$$\frac{I_{ansae} - I_{70°}}{I_{ansae}}$$

is given in Table III for several smearing widths and several ring-plane inclinations and indicates that the method was quite sensitive to variations in the smearing parameter. The model also showed that smearing of the planet itself was important throughout the portion of the ring which crossed the disk. This region coincides with the constant intensity portion of the observed brightness profile. Thus, smearing alone can adequately reproduce the observed brightness variations with orbital phase angle in Ring B, and we conclude that there are no intrinsic variations greater than 1 or 2 percent.

In an effort to check our interpretation of the observations of Ring B the observed data were smoothed and then divided by the scan given by the smeared model. The result of this operation is shown in Fig. 4. The curve produced by the ratio may be interpreted as a first approximation to the intrinsic ring profile, and it is evident that the ring is of uniform brightness within the uncertainty produced by the photometric noise.

This ring model was also used to investigate the change in the amplitude of this effect in Ring B with ring-plane inclination. Table III shows that the smearing process will cause a brightness decrease of over 20 percent when the inclination angle is less than 10 degrees. This agrees well with the data of Camichel (1958) which indicated a diminution of about 20 percent at small inclination angles.

A similar analysis of Ring C confirms our observations of a decrease in intensity from the minor axis towards the ansae. This is the expected result, since the observed brightness of Ring C is strongly influenced by the light scattered inward by seeing from Ring B.

Obviously, a simple smearing explanation will not suffice for Ring A, for the smearing process is incapable of producing a brightness distribution which is not symmetric about the major axis of the ring system. Illumination of the rings by sunlight scattered from Saturn is similarly unacceptable because of the lack of bilateral symmetry in the observed variations.

We have derived a representation of the intrinsic azimuthal variation of Ring A by the same method that was used for Ring B. Figure 5 illustrates the result of this de-smearing process. A narrow minimum occurs at an orbital phase angle of 70° with the subsequent broad

maximum appearing near 160°. The position of the maximum is subject to uncertainty for two reasons. First, the maximum is not sharp and is therefore difficult to locate and secondly, the region beyond 160° is confused due to the proximity of the image of the planet in the region from 160° to 200°. This pattern repeats itself on the other half of the ring system and is present at all radii in Ring A.

The reliability of the de-smearing process was demonstrated by altering the ring model to fit the derived azimuthal variation of Ring A and then smearing the new model. The resulting scan reproduced the data scan to within one percent of the intensity of Ring A except for the regions near the minor axis of the ring ellipse where smearing from the polar regions of Saturn is important.

The symmetry of this brightness variation would suggest that it is caused by synchronously-rotating particles, and that the observed photometric effect is due either to some peculiar geometry associated with the synchronously-locked particles or to systematically variable albedo distributions which are common to many or most of the particles. Both of these possible interpretations have been examined and will be reported in detail in a later paper. In general, however, we find the geometrical explanation unworkable and, instead, lean toward a model in which we have systematic albedo variations caused by preferential deposition of high-albedo material on relatively large, gravitationally-locked particles. Differential deposition might be caused by the finite size of the gravitationally-locked particles, where small particles orbiting at lesser radii would overtake the inner, trailing quadrant of a larger particle, which in turn would overtake the small-particle material at greater

radii and deposit it on the outer leading quadrant. This would alter the photometric properties of the exposed quadrant. The observed variations are qualitatively reproduced if the deposited material has a higher albedo than the large synchronously-rotating particles. It should be noted that this interpretation of the brightness variation of Ring A requires that a significant portion of the reflected light is scattered from the surface of large particles. Presumably similar variations are not observed in Ring B because its larger optical thickness increases the importance of multiple scattering, thereby reducing the effect of the albedo variations.

IV. SUMMARY

We have developed a photographic reduction process which allows the determination of the relative intensities of precisely positioned points in the image of Saturn with a photometric reliability of 3 percent. Using this method, we have examined the surface brightness of the ring system and find significant variations of brightness with orbital phase angle. In Ring B the brightness at a fixed radius decreases from each ansa towards the minor axis of the ring ellipse. Ring A shows a more complex behavior in which the first and third quadrants are darker than the second and fourth. This variation in Ring A amounts to nearly 10 percent and can be detected visually on high-quality prints of Saturn. In view of this fact it is surprising that visual observers apparently have not reported the effect.

Because atmospheric and photographic smearing play a dominant role in photometric observations of the ring system, the effects were simulated

by a computational model. This calculation performed the numerical equivalent of the smearing on an assumed brightness distribution of the rings, thereby permitting the determination of an unsmeared ring brightness distribution which, when smeared, matches the data. While this ring model does not represent the true ring in detail, it does provide the basis for further study of the effects of smearing in the ring image. Using this model, we find that the brightness variation observed in Ring B is adequately explained as a result of the increasing effect of smearing as the ring narrows towards the minor axis. For Ring A we derive the intrinsic ring variations which give rise to the observations. On the basis of the symmetry of this variation and its permanence at varying phase angles, we conclude that the source of the effect is albedo variations over the surface of large, synchronously-rotating ring particles.

ACKNOWLEDGMENTS

We are pleased to thank Sacramento Peak Observatory for the use of the microphotometer system. The photographs used in this study were taken by C. F. Knuckles and A. S. Murrell.

This work was supported by NASA Grants NGL-32-003-001 (RFB), NGL-03-002-002 (BAS), and the New Mexico State University Physical Science Laboratory (HJR).

REFERENCES

Beebe, R. F. (1976). Contr. New Mexico St. Univ. Obs. *1*, No. 4.

Camichel, H. (1958). Ann. d' Ap. *21*, 231.

Cook, A. F., Franklin, F. A., and Palluconi, F. D. (1973). Icarus *18*,317.

Coupinot, G. (1973). Icarus *19*, 212.

Ferrin, I. R. (1974). Icarus *22*, 159.

Franklin, F. A., and Cook. A. F. (1965). Astron. J. *70*, 704.

Lumme, K. (1975). Icarus *24*, 483.

Morrison, D. (1974). Icarus *22*, 57.

Price, M. J., and Baker, A. (1975). Icarus *25*, 136.

Reese, E. J. (1972). Icarus *15*, 466.

Table I. Photographic plate data.

Plate No.	Date	Color	B[a]	α
B-				
13229	5 Nov 72	Blue	-26°39	-3°8
13232		Green		
13233		Red		
13318	7 Dec 72	Green	-26.39	-0.3
13445	19 Jan 73	Red	-26.40	+4.4
13446		Blue		
13447		Green		
13448		UV		
13450		IR		
17583	13 Dec 74	Blue	-24.09	-2.8
17833	25 Feb 75	Red	-25.37	+5.1
17834		Green		
17839		Green		
17840		Red		
17844		Red		
17845		Green		
17847		Red		
17887	19 Mar 75	Red	-25.47	+6.1
17891		Red		
17892		Red		

[a]Saturnicentric latitude of the Earth

Table II. Ring model.

Ringlet	Boundary[a]	Intensity
	67.7	
B1		0.68
	72.6	
B2		0.90
	78.1	
B3		1.00
	85.4	
Cassini Division		0.24
	89.2	
A1		0.67
	93.4	
A2		0.50
	100	

[a]Boundary radius in percent of the ring system semi-major axis.

Table III. Brightness variation for Ring B.

	Inclination		
l/h	10°	18°	26°
0.4	22	8	3
0.5	24	11	6
0.6	26	17	9

FIGURE CAPTIONS

Fig. 1. Observed surface brightness of Ring B at 0.805 of the outer radius of the ring system. The lower tracing is relative intensity while the upper is fractional deviation from the mean intensity described in the text. Vertical lines mark the points at which the scan becomes influenced by the light from Saturn.

Fig. 2. Surface brightness as in Fig. 1 for Ring A at 0.919 of the outer radius.

Fig. 3. Major axis ring profile. a) The model ring cross-section and the profile resulting from smearing the model with a two-dimensional Gaussian function with a 0.5 arc-second halfwidth. b) Comparison of the smeared model profile (solid line) with the observations of the western ansa of plate B13447 (dots). c) As in b) for the eastern ansa.

Fig. 4. Azimuthal variation of Ring B (radius = 0.805). a) Normalized observed intensity plotted as a function of orbital phase angle. b) Normalized relative intensity as predicted by the smearing model. c) The ratio of the data scan and the model scan showing the de-smeared ring brightness variation.

Fig. 5. Azimuthal variation of Ring A (radius = 0.919). a),b),c) as in Fig. 4.

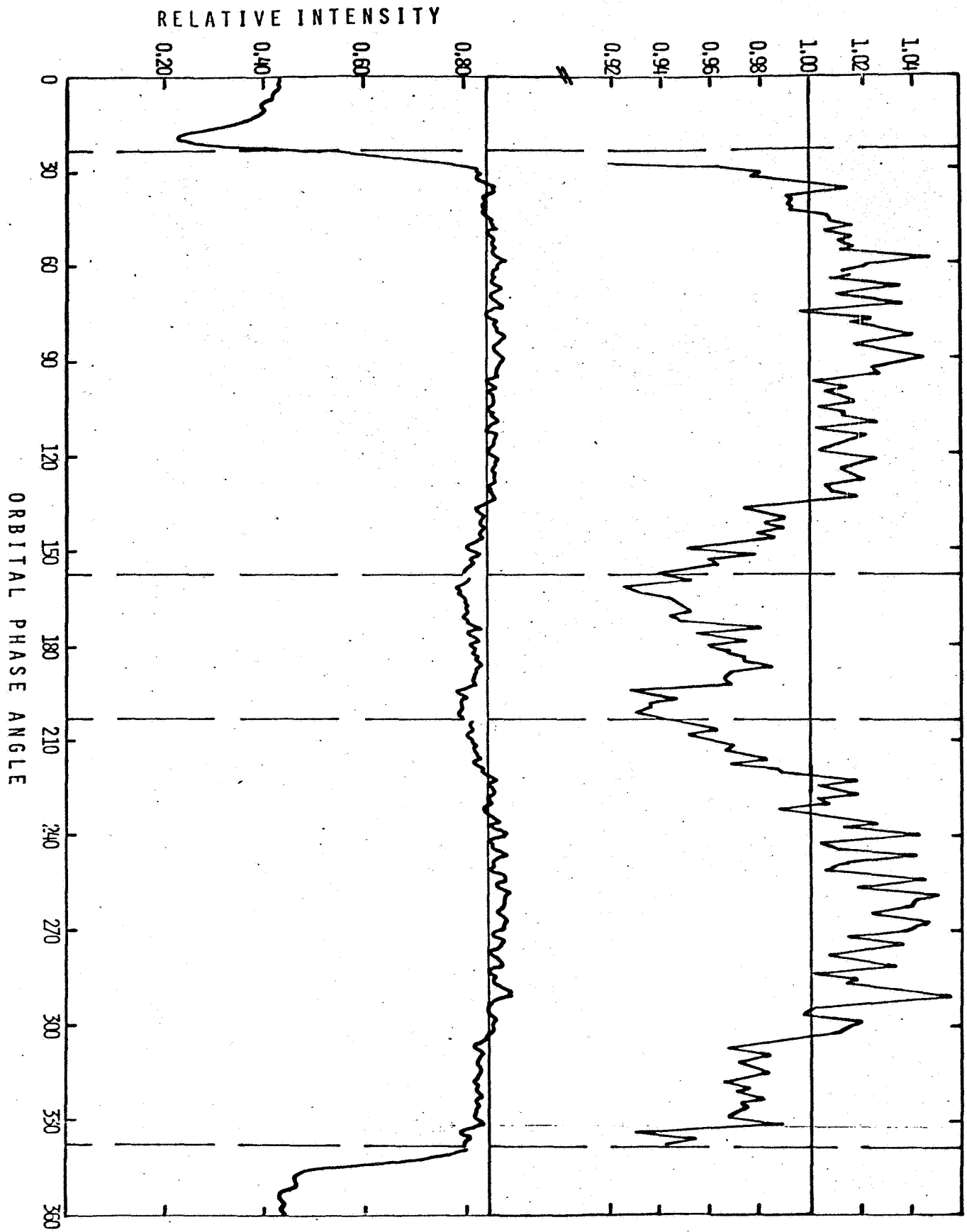

REITSEMA, BEEBE, SMITH, FIG. 1

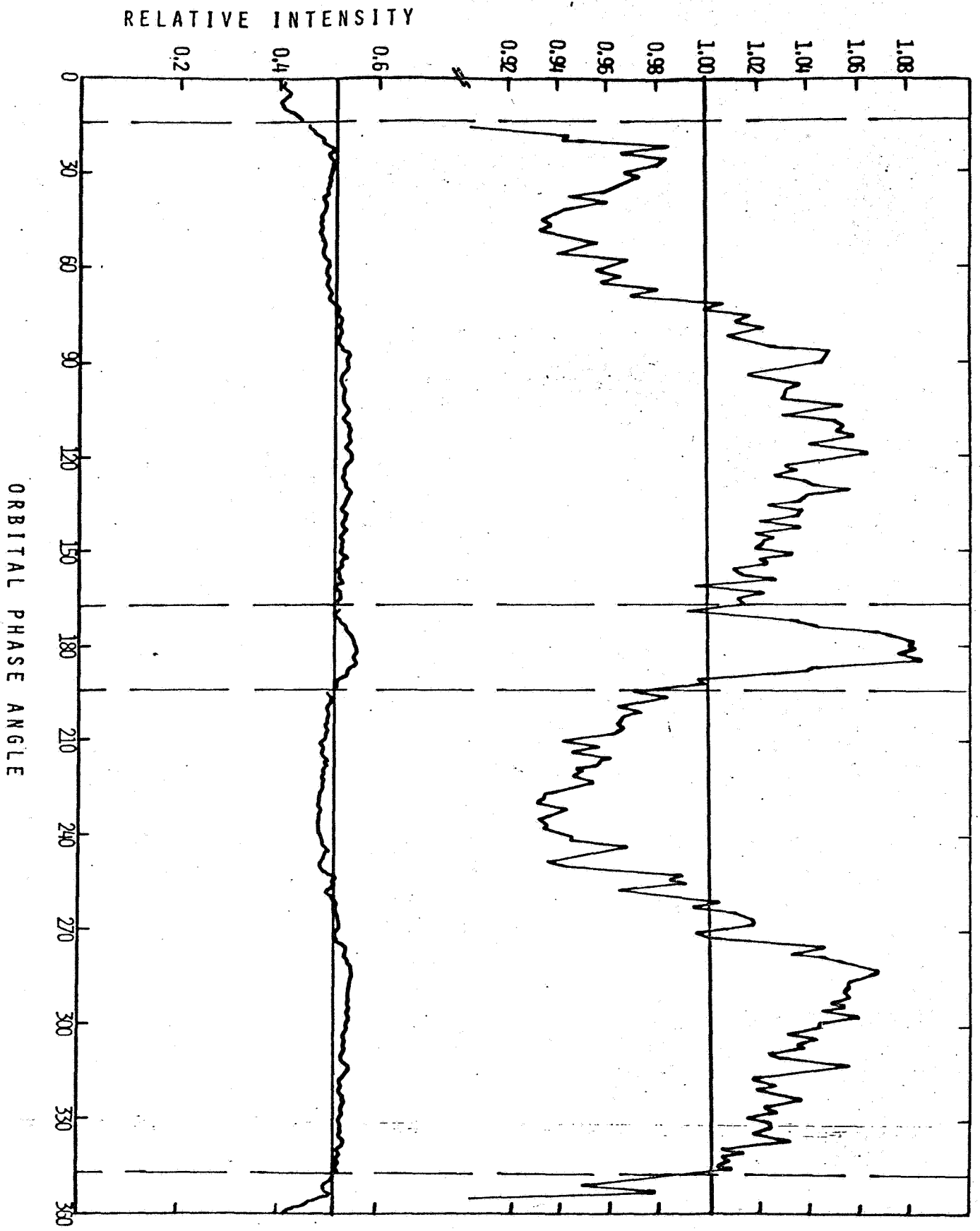

REITSEMA, BEEBE, SMITH FIG. 2

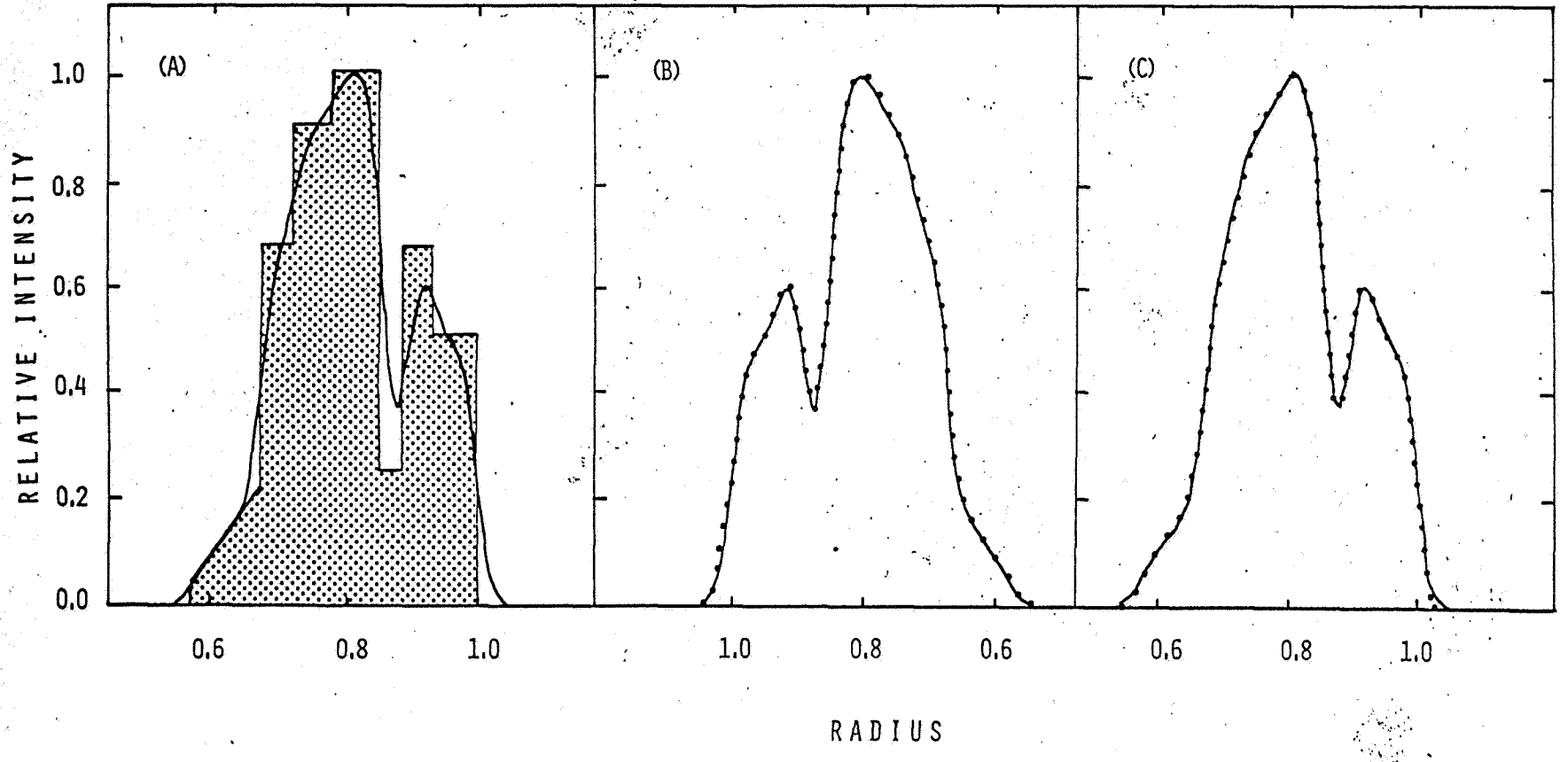

REITSEMA, BEEBE, SMITH, FIG. 3

REITSEMA, BEEBE, SMITH, FIG. 3

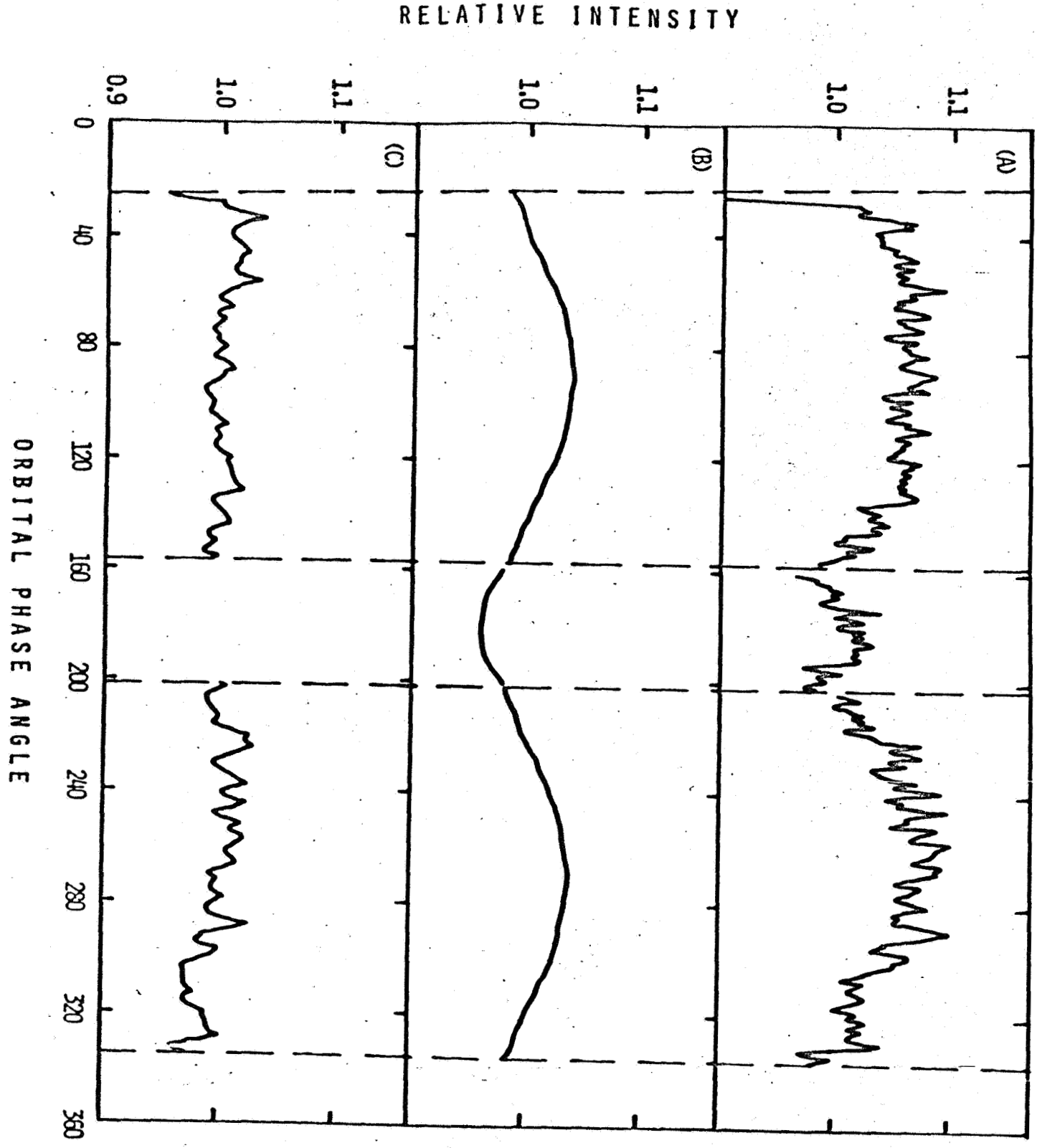

REITSEMA, BEEBE, SMITH, FIG. 4

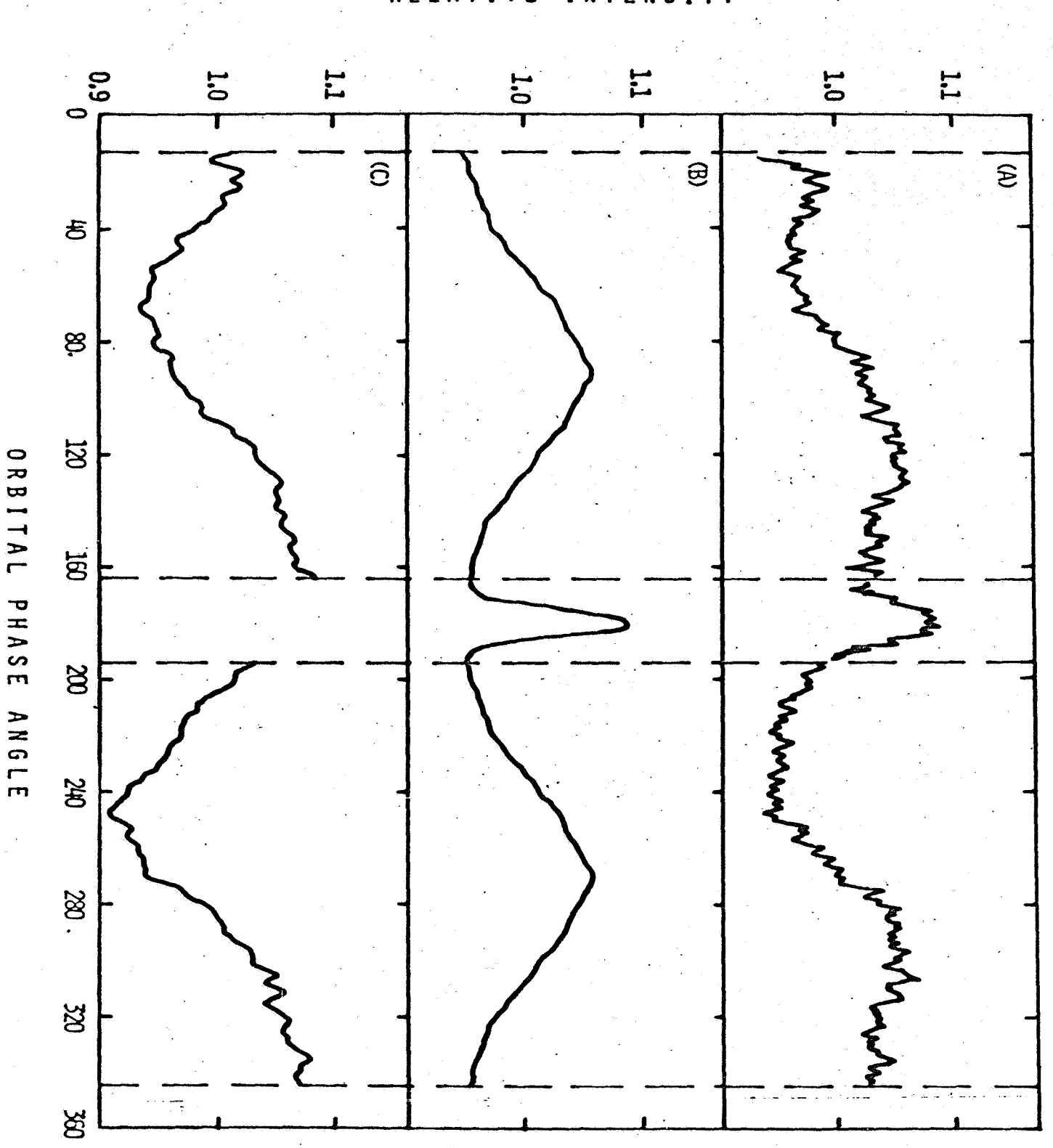

REITSEMA, BEEBE. SMITH. FIG 5